

RECENT DEVELOPMENTS IN THE DYNAMICAL AND UNITARY ISOBAR MODELS FOR PION ELECTROMAGNETIC PRODUCTION

SHIN NAN YANG AND GUAN YEU CHEN

Department of Physics, National Taiwan University, Taipei, Taiwan

S. S. KAMALOV

Laboratory of Theoretical Physics, JINR, 141980 Dubna, Russia

D. DRECHSEL AND L. TIATOR

Institut für Kernphysik, Universität Mainz, 55099 Mainz, Germany

$\gamma^*N\Delta$ transition form factors and threshold π^0 photo- and electroproduction are studied with the new version of MAID and a dynamical model. By re-analyzing the recent Jlab data on $p(e, e'p)\pi^0$ at $Q^2 = 2.8$ and 4.0 $(\text{GeV}/c)^2$, we find that the hadronic helicity conservation is not yet observed in this region of Q^2 . The extracted R_{EM} , starting from a small and negative value at the real photon point, actually exhibits a clear tendency to cross zero and change sign as Q^2 increases, while the absolute value of R_{SM} is strongly increasing. Our analysis indicates that $A_{1/2}$ and $S_{1/2}$, but not $A_{3/2}$, starts exhibiting the pQCD scaling behavior at about $Q^2 \geq 2.5$ $(\text{GeV}/c)^2$. For the π^0 photo- and electroproduction near threshold, results obtained within the dynamical model with the use of a meson-exchange πN model for the final state interaction are in as good agreement with the data as ChPT.

1 Introduction

Pion photo- and electroproduction reactions are powerful tools to probe the nucleon structure. The most prominent example is the $\Delta(1232)$ which decays almost exclusively into πN channel. The interest there lies in the possibility of observing deformation in the Δ . A deformed Δ would indicate that the Δ contains a D-state and the photon can excite a nucleon through electric $E2$ and Coulomb $C2$ quadrupole transitions. The study of $E_{1+}^{(3/2)}$ and $S_{1+}^{(3/2)}$ multipoles is expected to shed light on the structure of the nucleon and its first excited state. Recent experiments¹ give a nonvanishing ratio $R_{EM} = E_{1+}^{(3/2)}/M_{1+}^{(3/2)}$ between magnetic dipole $M_{1+}^{(3/2)}$ and electric quadrupole $E_{1+}^{(3/2)}$ multipoles lying between -2.5% and -3.0% at $Q^2 = 0$. In addition, the reaction $p(e, e'p)\pi^0$ provides us with the possibility of determining the range of photon four-momentum transfer squared Q^2 , where perturbative QCD (pQCD) would become applicable. In the limit of $Q^2 \rightarrow \infty$,

pQCD predicts the dominance of helicity-conserving amplitudes² and scaling results³. The hadronic helicity conservation would have the consequence that R_{EM} approaches 1. It is an intriguing question how R_{EM} would evolve from a very small negative value at $Q^2 = 0$ to +100% at sufficiently high Q^2 .

Another interesting issue is the π^0 photo- and electroproduction in the threshold region. At present time chiral perturbation theory (ChPT) is the basic theory for the description of these reactions in this energy region. It predicts a large one pion loop correction to the low energy theorem (LET) value of the E_{0+} multipole for the neutral pion photoproduction⁴. On the other hand the role of the one-pion loop correction can be related to the effect of final state interaction (FSI) developed within dynamical models^{5,6}. It is of interest to compare the predictions of these two different approaches.

In this talk, we present the results we have recently obtained with a new version (hereafter called MAID) of the unitary isobar model developed at Mainz⁷, and the dynamical model developed recently in Ref. ⁸ (hereafter called Dubna-Mainz-Taipei (DMT) model), both of which give excellent description of most of the existing pion photo- and electroproduction data, on the $\gamma^*N\Delta$ transition and the π^0 threshold production.

2 Formalism

We start with the description of the basic elements of our models. The main equation for the pion photo- and electroproduction t-matrix is

$$t_{\gamma\pi}(E) = v_{\gamma\pi} + v_{\gamma\pi} g_0(E) t_{\pi N}(E), \quad (1)$$

where $t_{\pi N}$ is the full pion-nucleon scattering matrix with total πN c.m. energy E and $g_0(E)$ is the free πN propagator.

In resonant channels like (3,3), the transition potential $v_{\gamma\pi}$ consists of two terms, $v_{\gamma\pi}(E) = v_{\gamma\pi}^B + v_{\gamma\pi}^R(E)$, where $v_{\gamma\pi}^B$ is the background transition potential and $v_{\gamma\pi}^R(E)$ corresponds to the contribution of the bare resonance. The resulting t-matrix can be expressed as a sum of two terms⁸,

$$t_{\gamma\pi} = t_{\gamma\pi}^B + t_{\gamma\pi}^R, \quad (2)$$

where

$$t_{\gamma\pi}^B = v_{\gamma\pi}^B + v_{\gamma\pi}^B g_0 t_{\pi N}, \quad t_{\gamma\pi}^R = v_{\gamma\pi}^R + v_{\gamma\pi}^B g_0 t_{\pi N}. \quad (3)$$

For physical multipoles in channel $\alpha = \{l, j\}$, Eq. (3) gives

$$t_{\alpha}^B(q_E, k; E + i\epsilon) = \exp(i\delta_{\alpha}) \cos \delta_{\alpha} \times \left[v_{\alpha}^B(q_E, k) + P \int_0^{\infty} dq' \frac{q'^2 R_{\alpha}(q_E, q') v_{\alpha}^B(q', k)}{E - E(q')} \right], \quad (4)$$

where δ_α and R_α are the πN scattering phase shift and reaction matrix, in channel α , respectively; q_E is the pion on-shell momentum and $k = |\mathbf{k}|$ is the photon momentum. The procedure which we use for the off-shell extrapolation and maintaining the gauge invariance is given in Ref. ⁸.

In the new version of MAID, the S , P , D and F waves of the t_α^B amplitude is defined in accordance with the K-matrix approximation

$$t_\alpha^B(\text{MAID}) = \exp(i\delta_\alpha) \cos \delta_\alpha v_\alpha^B(q, W, Q^2), \quad (5)$$

where $W \equiv E$ is the total πN c.m. energy. From Eqs. (4) and (5), one finds that the difference between the background terms of MAID and DMT models is that pion off-shell rescattering contributions (principal value integral) are not included in the MAID's background term.

3 Pion photo- and electroproduction in the $\Delta(1232)$ region

For the resonance contribution t_α^R in Eq. (3), the following Breit-Wigner form is assumed⁷ in both models,

$$t_\alpha^R(W, Q^2) = \bar{\mathcal{A}}_\alpha^R(Q^2) \frac{f_{\gamma R}(W) \Gamma_R M_R f_{\pi R}(W)}{M_R^2 - W^2 - i M_R \Gamma_R} e^{i\phi_R}, \quad (6)$$

where $f_{\pi R}$ is the usual Breit-Wigner factor describing the decay of resonance R with total width $\Gamma_R(W)$ and physical mass M_R . The phase $\phi_R(W)$ in Eq. (6) is introduced to adjust the phase of t_α^R to have the correct phase δ_α .

The main subject of our study in the resonance region is the strengths of the electromagnetic transitions described by amplitudes $\bar{\mathcal{A}}_\alpha^R(Q^2)$. In general, they are considered as free parameters to be extracted from analysis of the experimental data. In the present talk we will consider only results pertinent to the $\Delta(1232)$ resonance. In this case we impose the following parametrization for the electric ($\alpha = E$), magnetic ($\alpha = M$) and Coulomb ($\alpha = S$) amplitudes

$$\bar{\mathcal{A}}_\alpha^\Delta(Q^2) = X_\alpha^\Delta(Q^2) \bar{\mathcal{A}}_\alpha^\Delta(0) \frac{k}{k_W} F(Q^2), \quad (7)$$

where $k_W = (W^2 - m_N^2)/2W$. The form factor F is taken to be $F(Q^2) = (1 + \beta Q^2) e^{-\gamma Q^2} G_D(Q^2)$, where $G_D(Q^2) = 1/(1 + Q^2/0.71)^2$ is the usual dipole form factor. The values of $\bar{\mathcal{A}}_M^\Delta(0)$ and $\bar{\mathcal{A}}_E^\Delta(0)$ are obtained by setting $X_\alpha(0) = 1$ and fitting the pion photoproduction data. The parameters β and γ can be determined by setting $X_M^\Delta = 1$ and fitting the $\bar{\mathcal{A}}_M^\Delta(Q^2)$ to the existing data for G_M^* form factor.

Note that the physical meaning of the resonant amplitudes in different models is different⁸. In MAID, background contribution does not contain

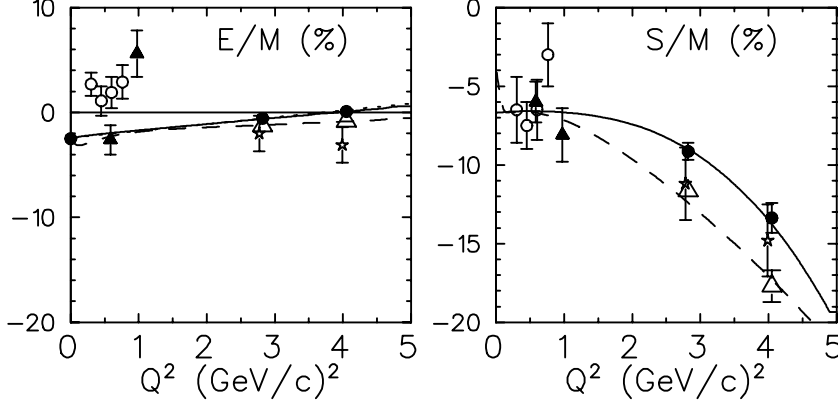


Figure 1. The Q^2 dependence of the ratios $R_{EM}^{(p\pi^0)}$ and $R_{SM}^{(p\pi^0)}$ at $W = 1232$ MeV. The solid and dashed curves are the MAID and DMT models results, respectively, obtained with a violation of the scaling assumption. Data at $Q^2 = 2.8$ and 4.0 (GeV/c) 2 are from Ref. ⁹ (stars). Results of our analysis at $Q^2 = 2.8$ and 4.0 (GeV/c) 2 are obtained using MAID (\bullet) and the DMT models (Δ). Other data are the same as in Ref. ⁸.

effects from the off-shell pion rescattering. Instead, they are effectively included in the resonance amplitude and it leads to the dressing of $\bar{A}_\alpha^\Delta(Q^2)$. Thus, using MAID we can extract information about so the called "dressed" $\gamma N\Delta$ vertex. However, in the dynamical model the background excitation is included in t_α^B and the electromagnetic vertex $\bar{A}_\alpha^\Delta(Q^2)$ corresponds to the "bare" vertex.

We determine the Q^2 dependence both for X_E and X_S , normalized to 1 at $Q^2 = 0$, from the recent $p(e, e'p)\pi^0$ experiment⁹ at $Q^2 = 2.8$ and 4.0 (GeV/c) 2 . Note that deviations from $X_\alpha^\Delta = 1$ value at finite Q^2 will indicate a violation of the scaling law. The extracted Q^2 dependence of the X_α^Δ parameters is $X_E^\Delta(\text{MAID}) = 1 - Q^2/3.7$, $X_E^\Delta(\text{DMT}) = 1 + Q^4/2.4$, and for the Coulomb $X_S^\Delta(\text{MAID}) = 1 + Q^6/61$, $X_S^\Delta(\text{DMT}) = 1 - Q^2/0.1$. The obtained R_{EM} and $R_{SM} = S_{1+}^{(3/2)}/M_{1+}^{(3/2)}$ ratios are compared with other's results in Fig. 1. The main difference between our results and those of Ref. ⁹ is that our values of R_{EM} show a clear tendency to cross zero and change sign as Q^2 increases. This is in contrast with the results obtained in the original analysis⁹ of the data which concluded that R_{EM} would stay negative and tends toward more negative value with increasing Q^2 . Furthermore, we find that the absolute value of R_{SM} is strongly increasing.

Finally in Fig. 2, we show our results for $Q^3 A_{1/2}$, $Q^5 A_{3/2}$, and $Q^3 S_{1/2}$ to check the scaling behavior predicted by pQCD: $A_{1/2} \sim Q^{-3}$, $A_{3/2} \sim Q^{-5}$ and

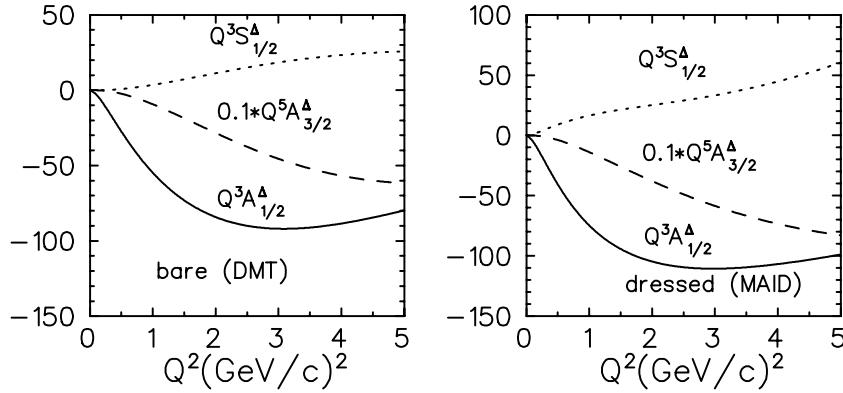


Figure 2. Asymptotic pQCD behaviors for the $A_{1/2}$, $A_{3/2}$ and $S_{1/2}$ helicity amplitudes obtained with DMT (left figure) and MAID (right figure).

$S_{1/2}^{(1/2)} \sim Q^{-3}$. It is interesting to see that both the bare $A_{1/2}$ and $S_{1/2}$ clearly starts exhibiting the pQCD scaling behavior at about $Q^2 \geq 2.5 (GeV/c)^2$, while $A_{3/2}$ does not. From these results, one might be tempted to speculate that scaling will set in earlier than the helicity conservation as predicted by pQCD.

4 Threshold π^0 photoproduction

Let us start with the π^0 photoproduction in the threshold region. Since the reaction can proceed through the $\pi^0 p$ and $\pi^+ n$ intermediate states, we may write π^0 photoproduction t-matrix as

$$\begin{aligned}
 t_{\gamma\pi^0}(E) = & v_{\gamma\pi^0}^B + v_{\gamma\pi^0}^B g_{\pi^0 p}(E) t_{\pi^0 p \rightarrow \pi^0 p}(E) \\
 & + v_{\gamma\pi^+}^B g_{\pi^+ n}(E) t_{\pi^+ n \rightarrow \pi^0 p}(E), \quad (8)
 \end{aligned}$$

where $t_{\pi^0 p \rightarrow \pi^0 p}$ and $t_{\pi^+ n \rightarrow \pi^0 p}$ are the πN scattering t-matrices for the elastic and charge exchange channels, respectively. They are obtained by solving coupled channels equations for the πN scattering using meson exchange model¹⁰. Results obtained in such an exact calculation and without the inclusion of FSI are depicted in Fig. 3 by dash-dotted and dotted curves, respectively. It clearly indicates that FSI effects is very important and brings the results into agreement with the data. We also find that the main FSI contribution (around 99%) comes from the principal value integral contribution in the charge exchange channel.

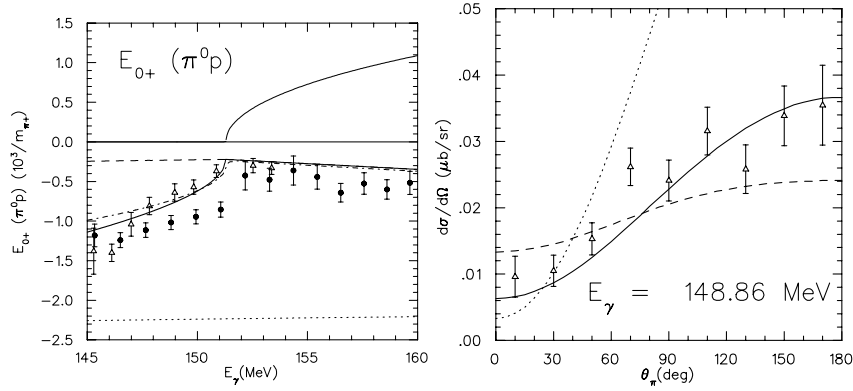


Figure 3. The E_{0+} multipole (left figure) and differential cross section (right figure) for the π^0 photoproduction on the proton. Dotted curves are the results obtained without FSI. Dash-dotted and solid curves are the results obtained with coupled-channels and K-matrix approaches, respectively. Dashed curve is the result without cusp effect. Data points are from Ref. ¹²(Δ) and Ref. ¹³(\bullet)

On the other hand, if the FSI effect is evaluated with the assumption of isospin symmetry (IS), i.e., with averaged masses in the free πN propagator, then the energy dependence in $Re E_{0+}$ near threshold would be smooth as given in the dashed curve of Fig. 3. Below π^+ threshold the strong energy dependence (cusp effect) appears only due to the pion mass difference and, as mentioned above, it arises mostly from the coupling with the charge exchange channel. In the literature, effects from the pion-mass difference below π^+ production channel has been taken into account using K-matrix approach^{4,11},

$$Re E_{0+}^{\gamma\pi^0} = Re E_{0+}^{\gamma\pi^0}(IS) - a_{\pi N} \omega_c Re E_{0+}^{\gamma\pi^+}(IS) \sqrt{1 - \frac{\omega^2}{\omega_c^2}}, \quad (9)$$

where ω and ω_c are the π^+ c.m. energies corresponding to the $W = E_p + E_\gamma$ and $W_c = m_n + m_{\pi^+}$, respectively. $a_{\pi N} = 0.124/m_{\pi^+}$ is the pion charge exchange amplitude, and $E_{0+}^{\gamma\pi^{0,+}}(IS)$ is the π^0 and π^+ photoproduction amplitude at threshold obtained without pion mass difference using Eq. (4). The corresponding results are given by the solid curves in Fig. 3. We can see that above π^+ threshold difference between results obtained in coupled-channels calculation and K-matrix approach is very small. This is consistent with the finding of Ref. ¹¹. At lower energies the difference became visible only very close to the $\pi^0 p$ threshold and it is around 10%. In general, we can conclude that Eq. (9) is a good approximation for the pion-mass difference effect. The

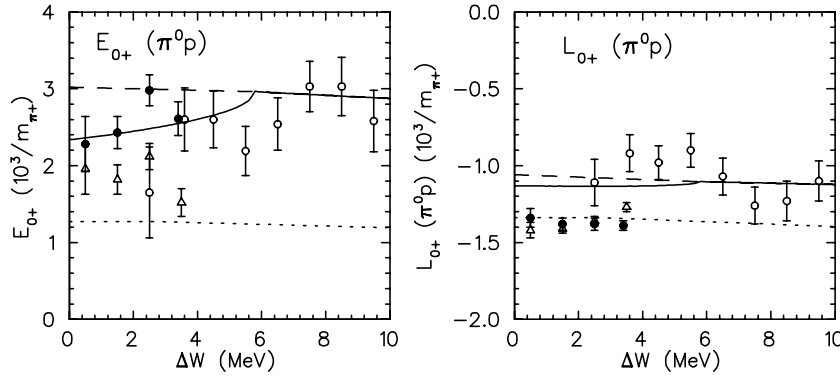


Figure 4. Real parts of the E_{0+} (left figure) and L_{0+} (right figure) multipoles for the π^0 electroproduction on the proton at $Q^2=0.1$ $(\text{GeV}/c)^2$. Notations for the curves are the same as in Fig. 1. Data points are from Ref.¹⁴(\circ) and Ref.¹⁵(Δ). Results of the present work obtained using p -waves from the DMT model are given by (\bullet).

threshold energy dependence for imaginary part can be easily obtained via Fermi-Watson theorem if in the threshold region πN phase shift is taken as a linear function of the π^+ momentum, i.e. they approaches 0 at $q_{\pi^+} \rightarrow 0$.

In Fig. 3, we also compare our prediction for the differential cross section with the data from Mainz¹². We see that both the off-shell pion rescattering and cusp effects substantially improve agreement with the data. Moreover it indicates that our model, without any new free parameter, also gives reliable predictions for the p -waves threshold behaviour.

5 Threshold π^0 electroproduction

Pion electroproduction provides us with information on the Q^2 dependence of the transverse E_{0+} and longitudinal L_{0+} multipoles in the threshold region. The "cusp" effects in L_{0+} multipole is taken into account in a similar way as in the case of E_{0+} ,

$$\text{Re } L_{0+}^{\gamma\pi^0} = \text{Re } L_{0+}^{\gamma\pi^0}(IS) - a_{\pi N} \omega_c \text{Re } L_{0+}^{\gamma\pi^+}(IS) \sqrt{1 - \frac{\omega^2}{\omega_c^2}}. \quad (10)$$

At threshold, the Q^2 dependence is given mainly by the Born + vector mesons contributions in $v_{\gamma\pi}^B$, as described in Ref. ⁷. In Fig. 4 we show our results for the cusp and FSI effects in E_{0+} and L_{0+} multipoles for the π^0 electroproduction at $Q^2 = 0.1$ $(\text{GeV}/c)^2$, along with the results of the multipole analysis from NIKHEF¹⁴ and Mainz¹⁵. Note that results of both groups were obtained

using the p -wave predictions given by ChPT. We have made a new analysis of the Mainz data¹⁵ for the differential cross sections, using our DMT p -wave multipoles instead. The s -wave multipoles extracted this way are also shown in Fig. 2 (solid circles). Note that results of our new analysis for the E_{0+} multipole are closer to the NIKHEF data and in better agreement with DMT model prediction. However, the results for the longitudinal L_{0+} multipole stay practically the same as in the previous Mainz analysis. We see that in this case DMT model prediction is in better agreement with the NIKHEF data.

In Fig. 5, DMT model predictions (dashed curves) are compared with the Mainz experimental data for the unpolarized cross sections $d\sigma/d\Omega = d\sigma_T/d\Omega + \epsilon d\sigma_L/d\Omega$, and longitudinal-transverse cross section $d\sigma_{TL}/d\Omega$. Overall, the agreement is good. If the L_{0+} multipole in DMT model is replaced with that extracted from Mainz data, then the agreement with the Mainz data is further improved as given by the solid curves in Fig. 5.

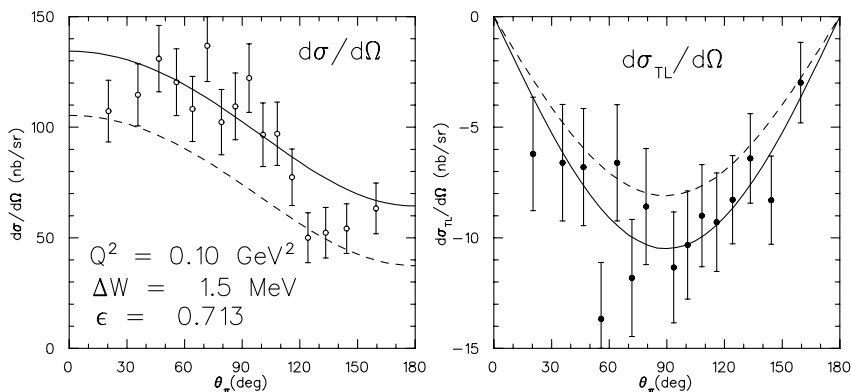


Figure 5. Angular distribution $d\sigma/d\Omega = d\sigma_T/d\Omega + \epsilon d\sigma_L/d\Omega$, for the π^0 electroproduction on the proton at $Q^2=0.1$ $(\text{GeV}/c)^2$, $\epsilon = 0.713$ and at total c.m. energies $\Delta W = W - W_{thr}^{\pi^0 p} = 1.5$ MeV. Dashed curves are the predictions of the DMT model. Solid curves are our results of the local fit with fixed p -waves. Experimental data from Ref.¹⁵.

6 Conclusion

In summary, the $\gamma^* N\Delta$ transition form factors and threshold π^0 photo- and electroproduction are studied with the new version of MAID and a dynamical model. By re-analyzing recent Jlab data on $p(e, e'p)\pi^0$ at $Q^2 = 2.8$ and 4.0 $(\text{GeV}/c)^2$, we find that $A_{3/2}$ is still as large as $A_{1/2}$ at $Q^2 = 4$ $(\text{GeV}/c)^2$,

which implies that hadronic helicity conservation is not yet observed in this region of Q^2 . Accordingly, our extracted values for R_{EM} are still far from the pQCD predicted value of +100%. However, in contrast to previous results we find that R_{EM} , starting from a small and negative value at the real photon point, actually exhibits a clear tendency to cross zero and change sign as Q^2 increases, while the absolute value of R_{SM} is strongly increasing. In regard to the scaling, our analysis indicates that $A_{1/2}$ and $S_{1/2}$, but not $A_{3/2}$, starts exhibiting the pQCD scaling behavior at about $Q^2 \geq 2.5(GeV/c)^2$. It appears likely that the onset of scaling behavior might take place at a lower momentum transfer than that of hadron helicity conservation. For the π^0 photo- and electroproduction near threshold, results obtained within the dynamical model with the use of a meson-exchange πN model for the final state interaction are in as good agreement with the data as ChPT.

References

1. R. Beck *et al.*, Phys. Rev. Lett. **78**, 606 (1997); G. Blanpied *et al.*, Phys. Rev. Lett. **79**, 4337 (1997).
2. S.J. Brodsky and G.P. Lepage, Phys. Rev. D **23**, 1152 (1981); *ibid.* **24**, 2848 (1981).
3. C.E. Carlson, Phys. Rev. D **34**, 2704 (1986); C.E. Carlson and N.C. Mukhopadhyay, Phys. Rev. Lett. **81**, 2446 (1998).
4. V. Bernard, J. Gasser, N. Kaiser, and U.-G Meissner, Phys. Lett. **B268**, 291 (1991); Z. Phys. **C70**, 483 (1996).
5. S. N. Yang, Phys. Rev. C **40**, 1810 (1989); C. Lee, S. N. Yang, and T.-S. H. Lee, J. Phys. G: Nucl. Part. Phys. **17**, L131 (1991).
6. S. Nozawa, T.-S.H. Lee, and B. Blankleider, Phys. Rev. C **41**, 213 (1990).
7. D. Drechsel, O. Hanstein, S.S. Kamalov and L. Tiator, Nucl. Phys. **A645**, 145 (1999).
8. S. S. Kamalov and S. N. Yang, Phys. Rev. Lett. **83**, 4494 (1999).
9. V.V. Frolov *et al.*, Phys. Rev. Lett. **82**, 45 (1999).
10. C. T. Hung, S.N. Yang, and T.-S.H. Lee, J. Phys. G20, 1531 (1994); to appear in Phys. Rev. C, 2001.
11. J. M. Laget, Phys. Rep. **69**, 1 (1981).
12. M. Fuchs *et al.*, Phys. Lett. **B368**, 20 (1996).
13. J. C. Bergstrom *et al.*, Phys. Rev. C **53**, R1052 (1996); *ibid.* 1509 (1997).
14. H.B. van den Brink *et al.*, Phys. Rev. Lett. **74**, 3561 (1995); Nucl. Phys. **A612**, 391 (1997).
15. M. O. Distler *et al.*, Phys. Rev. Lett. **80**, 2294 (1998).